Journal of Contaminant Hydrology 123 (2011) 40–49

Contents lists available at ScienceDirect

Journal of Contaminant Hydrology

journal homepage: www.elsevier.com/locate/jconhyd

Macrodispersion by diverging radial flows in randomly heterogeneous porous media

Gerardo Severino*, Alessandro Santini, Angelo Sommella

Division of Water Resources Management, University of Naples Federico II, Italy

ARTICLE INFO

Article history:
Received 2 August 2010
Received in revised form 16 December 2010
Accepted 17 December 2010
Available online 5 January 2011

Keywords:
Radial flow
Heterogeneity
Macrodispersion
Stochastic modelling

ABSTRACT

Radial flow takes place in a heterogeneous porous formation where the transmissivity T is modelled as a stationary *random space function* (RSF). The steady flow is driven by a given rate, and the mean velocity is radial. A pulse-like of a tracer is injected in the porous formation, and the thin plume spreads due to the fluctuations of the velocity which results a RSF as well. Transport is characterized by the mean front, and by the second spatial moment of the plume. We are primarily interested in tracer macrodispersion modelling.

With the neglect of pore-scale dispersion, macrodispersion coefficients are computed at the second order of approximation, without neglecting the head-gradient fluctuations. Although transport is non-ergodic at the source, it is shown that ergodicity is achieved at small distances from the source. This is due to the fact that close to the source local velocities are quite large, and therefore solute particles become uncorrelated very soon. Under ergodic conditions, we compare macrodispersion mechanism in radial flows with that occurring in mean uniform flows. At short distances the spreading effect is highly enhanced by the large variability of the flow field, whereas at large distances transport exhibits a lesser dispersion due to the reduction of velocities. This supports the explanation provided by Indelman and Dagan (1999) to justify why the macrodispersivity is found smaller than that pertaining to mean uniform flows.

The model is tested against a tracer transport experiment (Fernàndez-Garcia et al., 2004) by comparing the theoretical and experimental breakthrough curves. The accordance with real data, that is achieved without any fitting to concentration values, strengthens the capability of the proposed model to grasp the main features of such an experiment, the approximations as well as experimental uncertainties notwithstanding.

1. Introduction

Field tracer tests represent a practical site-specific technique for estimating aquifer parameters. Monitoring breakthrough curves of solutes injected into the subsurface provides information on the spreading processes influencing the plume migration. At aquifer scale, because the groundwater velocity is generally very small, it is a common practice to force the flow by using injecting/pumping well(s). Unlike flows driven by natural gradients, forced tests involve (as a rule) nonuniform mean flows. Notwithstanding this fundamental difference especially close to the release zone, aquifer parameters estimated from uniform and forced tests are often compared without distinction (Gelhar et al., 1992). Thus, macrodispersivity estimates obtained using forced tracer tests generally do not lead to the same values required to simulate the plume migration under natural flow conditions (Ptak et al., 2004). Even more dramatic are differences if one uses the uniform flow configuration to infer the statistical properties of an aquifer where flow is radial (Fernàndez-Garcia et al., 2004). Only recently a few theoretical studies on radial flows in the field of *Stochastic Hydrogeology* have been undertaken (a general overview can be found in Zhang, 2002; and Rubin, 2003).

* Corresponding author. Gerardo SEVERINO: University of Naples, via Università 100, 80055 Portici (NA)-ITALY. Tel./fax: +39 081 2539426(412).
E-mail address: severino@unina.it (G. Severino).

0169-7722/$ – see front matter © 2010 Elsevier B.V. All rights reserved.
doi:10.1016/j.jconhyd.2010.12.005

The theoretical bases to approach radial flows in heterogeneous porous media can be traced back to the pioneering studies of Shvidler (1966). Subsequently, Indelman and Abramovich (1994), and Indelman (2001) have further expanded results on source-flows in randomly heterogeneous porous formations. The approach developed in these studies allows statistical moments of flow variables to be derived (e.g. Fiori et al., 1998; Severino et al., 2008).

A general methodology for solving transport in heterogeneous formations can be found in Morales-Casique et al. (2006). The most important result is that large-scale transport parameters are nonlocal, and they depend on the flow configuration. Tracer macrodispersion in radial flow configurations has been theoretically tackled by Indelman and Dagan (1999) who have derived macrodispersion coefficients starting from the Lagrangian formulation of the transport problem. The major difference between transport in radial and uniform flow is that the large-time macrodispersivity in the former is smaller by a factor which increases with the flow domain dimensionality. To achieve a simple (analytical) solution, Indelman and Dagan (1999) proposed a major simplification consisting of neglecting in the velocity covariance the head-gradient fluctuations. While such an assumption is accurate at large distances from the source, it does not lend itself to investigations of macrodispersion in the vicinity of the source. From a practical point of view (due to logistic limitations) forced tracer tests quite often are carried out by monitoring the breakthrough curves at short distances from forcing well(s). As a consequence, the approximation of Indelman and Dagan (1999) should be used cautiously in the applications.

The objective of the present paper is to investigate advective transport in radial flow configurations. This is achieved at the first order of approximation in the variance σ_ε^2 of the normalized fluctuation $\varepsilon(\mathbf{x}) = 1-\frac{T(\mathbf{x})}{T_A}$ (T_A being the arithmetic mean). Unlike Indelman and Dagan (1999), we derive a complete analytical expression for the macrodispersion coefficient. This enables one to better quantify the spreading mechanism of tracers as well as the differences with results based on the approximation proposed by Indelman and Dagan (1999). Although our theoretical results in principle pertain to a two-dimensional formation, it is shown that they can be satisfactorily used to analyze a *divergent flow tracer test* provided that the hydraulic conductivity is properly up-scaled.

2. Problem formulation

A two-dimensional porous formation lies in an unbounded domain Ω. The hydraulic transmissivity $T(\mathbf{x})$ is modelled as a stationary RSF of the position $\mathbf{x}\in\Omega$ with arithmetic mean T_A, variance σ_T^2, and a given isotropic correlation function ρ_T. Flow is generated by a source-like (Dirac function) injection of water at constant specific volumetric rate Q (Fig. 1). The governing equation is

$$\nabla\cdot[T(\mathbf{x})\mathbf{E}(\mathbf{x})] = Q\delta(\mathbf{x}), \tag{1}$$

being $\mathbf{E}(\mathbf{x}) = -\nabla H(\mathbf{x})$ the head-gradient. A solution of the stochastic Eq. (1) is the RSF $H(\mathbf{x})$. As for transport, the tracer concentration (mass of tracer per liquid volume) $C(\mathbf{x},t)$ satisfies the advection–dispersion equation

$$\frac{\partial}{\partial t}C + \mathbf{u}\cdot\nabla C = \nabla\cdot(\mathbf{D}\nabla C) \tag{2}$$

where the Darcian velocity $\mathbf{u}(\mathbf{x})$ is defined as the ratio between the specific discharge $\mathbf{q}(\mathbf{x})$, and the porosity n (assumed constant). Finally, $\mathbf{D}$ is the pore-scale dispersion tensor. Due to the spatial variations of $T(\mathbf{x})$, the velocity $\mathbf{u}(\mathbf{x})$ fluctuates along flow paths, and concurrently the tracer-plume develops with a complex structure (Fig. 1). In many applications (e.g. Chao et al., 2000; Fernàndez-Garcia et al., 2004), the propagation of solute bodies is conveniently described by means of spatial moments of C (a general formulation can be found in Cvetkovic and Dagan, 1994). In particular, since we are concerned with a radial flow configuration, it is natural to use radial moments $S_{rr} = S_{rr}(t)$ to quantify the spreading mechanism.

The problem stated here in a general form is more complex than the similar one for mean uniform flows. A general overview on the technical difficulties is provided by Indelman and Dagan (1999). A simple solution can be achieved by making a few simplifying assumptions:

(i) a first order approximation (appropriate for mildly heterogeneous formations) is employed for calculating the head $H(\mathbf{x})$;
(ii) pore-scale dispersion is neglected in Eq. (2). In contrast, pore-scale dispersion plays an essential role in dilution since it significantly affects the variance of the concentration (see discussion in Lessoff and Indelman, 2004).

2.1. The flow field

We wish to compute the mean and two-point covariance of the velocity. By defining the zero mean RSF

$$\varepsilon(\mathbf{x}) = 1-\frac{T(\mathbf{x})}{T_A}, \tag{3}$$

and introducing it into (1) leads to

$$\Delta_2 H(\mathbf{x}) = -\nabla\cdot[\varepsilon(\mathbf{x})\mathbf{E}(\mathbf{x})]-\frac{Q}{T_A}\delta(\mathbf{x}). \tag{4}$$

To solve Eq. (4), the head is expanded into an asymptotic series $H(\mathbf{x}) = \sum_{i=0}^{n} H^{(i)}(\mathbf{x})$ with $H^{(i)} = \mathcal{O}(\varepsilon^i)$. Substituting the expansion into Eq. (4), and collecting terms up to the first order gives

$$\Delta_2 H^{(0)}(\mathbf{x}) = -\frac{Q}{T_A}\delta(\mathbf{x}), \qquad \Delta_2 H^{(1)}(\mathbf{x}) = -\nabla\cdot\left[\varepsilon(\mathbf{x})\mathbf{E}^{(0)}(\mathbf{x})\right]. \tag{5}$$

The head distribution $H^{(0)}$ represents the solution to the flow problem in a homogeneous formation, and it is given by:

$$H^{(0)}(\mathrm{x}) = -\frac{Q}{2\pi T_A}\ln\left(\frac{\mathrm{x}}{\ell_0}\right) \tag{6}$$

(being $\mathrm{x} = |\mathbf{x}|$). Because we are dealing with a potential flow, $H^{(0)}$ is uniquely determined by imposing the condition of its vanishing at a certain distance ℓ_0 from the source.

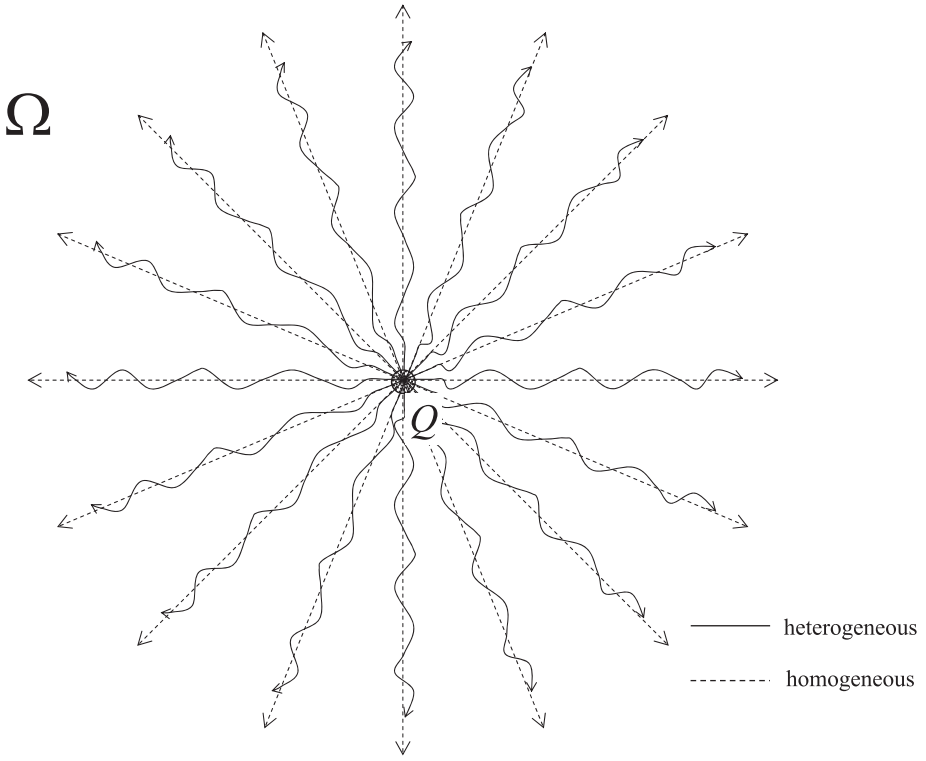

Fig. 1. Sketch illustrating the flow pattern generated by a source-like injection of water at given specific volumetric rate Q. Dashed lines represent the stream lines in a homogeneous medium, whereas continuous lines represent the stream lines as affected by the medium heterogeneity.

The head fluctuation $H^{(1)}(\mathbf{x})$ can be expressed in terms of the Green function $G(\mathrm{x}) = \frac{T_A}{Q}H^{(0)}(\mathrm{x})$ as

$$H^{(1)}(\mathbf{x}) = \frac{Q}{T_A}\int_\Omega d\mathbf{x}'\varepsilon(\mathbf{x}')\frac{\partial}{\partial x'_m}G(\mathrm{x}')\frac{\partial}{\partial x'_m}G(|\mathbf{x}-\mathbf{x}'|). \quad (7)$$

By the same token, we expand in asymptotic series the velocity **u**, and get the following equations for the various terms:

$$\mathbf{u}^{(0)}(\mathbf{x}) = \frac{T_A}{n}\mathbf{E}^{(0)}(\mathbf{x}), \qquad \mathbf{u}^{(i)}(\mathbf{x}) = \frac{T_A}{n}\left[\mathbf{E}^{(i)}(\mathbf{x}) - \varepsilon(\mathbf{x})\mathbf{E}^{(i-1)}(\mathbf{x})\right] \quad (8)$$

(with $i=1,2,..$). Since we are concerned with radial dispersion, hereafter we shall deal with the velocity covariance along radii, i.e. $u_{rr}(\mathbf{r}',\mathbf{r}'') = \langle u_r^{(1)}(\mathbf{r}')u_r^{(1)}(\mathbf{r}'')\rangle$ (being $u_r^{(1)}$ the fluctuation of the radial component u_r of the velocity), which is expressed as $u_{rr}(\mathbf{r}',\mathbf{r}'') = \left(\frac{T_A}{n}\right)^2\overline{u}_{rr}(\mathbf{r}',\mathbf{r}'')$ with

$$\overline{u}_{rr}(\mathbf{r}',\mathbf{r}'') = u_{rr}^{(\infty)}(\mathbf{r}',\mathbf{r}'') - \widetilde{u}_{rr}(\mathbf{r}',\mathbf{r}'') + C_{E_r}(\mathbf{r}',\mathbf{r}'') \quad (9)$$

$$u_{rr}^{(\infty)}(\mathbf{r}',\mathbf{r}'') = \left(\frac{\sigma}{\chi}\right)^2\frac{\rho(|\mathbf{r}'-\mathbf{r}''|)}{r'r''}, \quad (10)$$

$$\widetilde{u}_{rr}(\mathbf{r}',\mathbf{r}'') = \frac{1}{\chi}\left[\frac{1}{r'}\frac{\partial}{\partial r''}C_{\varepsilon H}(\mathbf{r}',\mathbf{r}'') + \frac{1}{r''}\frac{\partial}{\partial r'}C_{\varepsilon H}(\mathbf{r}'',\mathbf{r}')\right] \quad (11)$$

$\left(\chi = \frac{2\pi T_A}{Q}\right)$. The quantity $C_{E_r}(\mathbf{r}',\mathbf{r}'') = \left\langle\frac{\partial}{\partial r'}H^{(1)}(\mathbf{r}')\frac{\partial}{\partial r''}H^{(1)}(\mathbf{r}'')\right\rangle$ is the head-gradient covariance, whereas $C_{\varepsilon H}(\mathbf{r}',\mathbf{r}'') = \langle\varepsilon(\mathbf{r}')H^{(1)}(\mathbf{r}'')\rangle$ represents the cross-correlation between ε (and therefore T), and the head H.

The usefulness of the decomposition (Eq. (9)) relies on the fact that one can clearly distinguish the contribution due to the mean radial flow (i.e. $u_{rr}^{(\infty)}$) from those related to the head-gradient fluctuations. Computing $\widetilde{u}_{rr}(\mathbf{r}',\mathbf{r}'')$ and $C_{E_r}(\mathbf{r}',\mathbf{r}'')$ requires multi-dimensional numerical quadratures (see Fiori et al., 1998). This computational burden was circumvented by Indelman and Dagan (1999) who took advantage of the highly anisotropic geometry of sedimentary formations. Indeed, Indelman and Dagan (1999) showed that the velocity covariance (Eq. (9)) can be well approximated by retaining only the term $u_{rr}^{(\infty)}$. This assumption is also equivalent to approximating the velocity fluctuation $u_r^{(1)}(\mathbf{r})$ with

$$u_r^{(1)}(\mathbf{r}) \approx -\frac{T_A}{n}\varepsilon(\mathbf{r})E_r^{(0)}(r) \quad (12)$$

($E_r^{(0)}$ represents the head-gradient along the radial direction). Although Eq. (12) provides a systematic underestimation of the second order radial moment $S_{rr}(t)$, it leads to the same asymptotic macrodispersion coefficient $D_{rr}(\infty) = \frac{1}{2}\lim_{t\to\infty}\frac{d}{dt}S_{rr}(t)$ as in the complete case (see discussion in Indelman and Dagan, 1999).

However, the approximation of Indelman and Dagan (1999) may not be appropriate either from a theoretical or from a practical standpoint. Indeed, from the theoretical point of view the approximation (Eq. (12)) does not apply to isotropic formations, whereas from the practical point of view, in most of the forced tracer experiments (see, Chao et al., 2000; Fernàndez-Garcia et al., 2004; Ptak et al., 2004) breakthrough curves are monitored at distances relatively

short. In such cases a complete evaluation of the velocity covariance u_{rr} is required. Toward this aim, it is seen (Eq. (11)) that to evaluate $\widetilde{u}_{rr}$, it suffices to calculate the cross covariance $C_{\varepsilon H}$. This has been done (see the Appendix A for details) for an arbitrary autocorrelation ρ_ε with given finite integral scale I, and the final result is:

$$C_{\varepsilon H}(r',r'') = \frac{\sigma_\varepsilon^2}{\chi}\left[\int_{|r'-r''|}^{\infty}\frac{d\xi\,\xi\rho_\varepsilon(\xi)}{\xi^2-r'(r'-r'')} - \int_0^{r'}\frac{d\xi\,\xi\rho_\varepsilon(\xi)}{\xi^2-r'(r'-r'')}\right]. \tag{13}$$

Substitution into Eq. (11), and carrying out the required differentiations, leads to:

$$\widetilde{u}_{rr}(r',r'') = -2\overline{u}_{rr}^{(\infty)}(r',r'') - \left(\frac{\sigma_\varepsilon}{\chi}\right)^2\left[\Psi(r',r'') + \Psi(r'',r')\right] \tag{14}$$

$$\Psi(r',r'') = \int_{|r'-r''|}^{\infty}\frac{d\xi\,\xi\rho_\varepsilon(\xi)}{\xi^2-r'(r'-r'')} - \int_0^{r'}\frac{d\xi\,\xi\rho_\varepsilon(\xi)}{\xi^2-r'(r'-r'')} \tag{15}$$

(where $\overline{u}_{rr}^{(\infty)}(x,y) = u_{rr}^{(\infty)}(x,y)$ for $x \neq y$, and $\overline{u}_{rr}^{(\infty)}(x,x) = \frac{1}{2}u^{(\infty)}(x,x)$). As for the head-gradient covariance, it is equal (see the Appendix A) to

$$C_{E_r}(r',r'') = \overline{u}_{rr}^{(\infty)}(r',r'') + \left(\frac{\sigma_\varepsilon}{\chi}\right)^2\Psi(r',r''), \tag{16}$$

and finally the velocity-covariance writes as

$$u_{rr}(r',r'') = \left(\frac{\overline{Q}}{\pi}\right)^2\left[\frac{\rho_\varepsilon(r'-r'')}{r'r''} + \frac{1}{2}\Psi(r',r'') + \frac{1}{4}\Psi(r'',r')\right],\ \left(\overline{Q} = \frac{Q}{n}\sigma_\varepsilon\right). \tag{17}$$

The general result (Eq. (17)) expresses the two-point velocity covariance u_{rr} via one quadrature that is easily computed after specifying the shape of the autocorrelation function. In particular, Ψ is analytically derived for Gaussian ρ_ε the final result being

$$\Psi(r',r'') = \frac{\rho_\varepsilon(r')}{2r'r''} - \frac{r'\rho_\varepsilon(r'-r'')-r''}{2r'r''(r'-r'')} - \frac{\pi}{8}\exp\left[-\frac{\pi}{4}r'(r'-r'')\right]\overline{\Psi}(r',r'') \tag{18}$$

$$\overline{\Psi}(r',r'') = \mathrm{Ei}\left[-\frac{\pi}{4}r'(r''-r')\right] - \mathrm{Ei}\left[-\frac{\pi}{4}r''(r''-r')\right] - \mathrm{Ei}\left(-\frac{\pi}{4}r'r''\right). \tag{19}$$

The function $\mathrm{Ei}(-x) = -\int_x^\infty \frac{du}{u}\exp(-u)$ represents the exponential integral function. We have depicted (Fig. 2) $\frac{u_{rr}(r',r'')}{\overline{Q}^2}$ as computed from Eqs. (17) and (18) versus the distance $\frac{r'}{I}$ from the source, and different $\frac{r''}{I}$. The striking (in view of its impact upon macrodispersion modelling) result is that the rate of decaying (i.e. the slope) of the correlation is higher as $\frac{r''}{I}$ is smaller. This is explained by recalling that in the near-injection zone velocities of particles are very high, and therefore particles that initially are pretty close to the source will soon become uncorrelated. In a different way, one could say that the smaller (as compared with I) the characteristic size ℓ of the injecting area, the sooner the velocities of two particles will become uncorrelated, and *vice versa*.

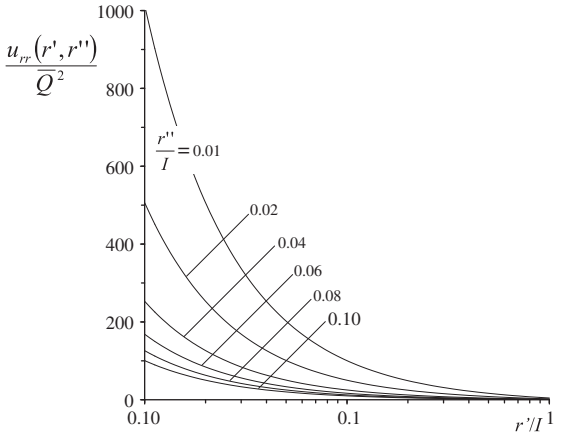

Fig. 2. Scaled velocity covariance $\frac{u_{rr}(r',r'')}{\overline{Q}^2}$ versus the distance $\frac{r'}{I}$, and different values of $\frac{r''}{I}$.

3. Macrodispersion analysis

Tracer transport in heterogeneous porous formations has been mainly studied by assuming the *ergodic hypothesis* (for a comprehensive exposition, see Rubin, 2003). For transport in mean uniform flows, the applicability of the ergodic hypothesis is bound to be satisfied if the length scale characterizing the initial size of the solute body is much larger than the heterogeneity scale I. In our case transport conditions differ from those pertaining to mean uniform flows. Thus, the salient question is: what is the role of a radial flow configuration upon attainment of ergodic conditions? The aim of the following sub-section is to investigate this issue along the lines of Dagan (1990).

3.1. Non-ergodic versus ergodic transport

A measure of tracer macrodispersion is given by the second order radial moment S_{rr}. By skipping the algebraic derivations (which can be found in Kitanidis, 1988; and Dagan, 1990), one obtains the fundamental relationship

$$S_{rr}(R,\ell) = S_{rr}(0,\ell) + X_{rr}(R,0) - \mathcal{R}_{rr}(R,\ell). \tag{20}$$

In words, the trajectory variance X_{rr} equals (up to the constant $S_{rr}(0,\ell)$ characterizing the initial spreading of the plume) to the sum of S_{rr}, and the variance of the plume centroid

$$\mathcal{R}_{rr}(R,\ell) = A_0^{-2}\iint d\mathbf{a}\,d\mathbf{b}\left\langle \overline{X}_r'(t;\mathbf{a})\overline{X}_r'(t;\mathbf{b})\right\rangle, \tag{21}$$

where $\overline{X}_r'$ represents the fluctuation of the displacement, and ℓ is a characteristic length of the release area A_0. Thus, the trajectory variance X_{rr} can be regarded as a measure of the spreading (see Eq. (20)) only when the variance of the plume centroid is exceedingly small, i.e. $\mathcal{R}_{rr} \approx 0$. In this case transport is coined as *ergodic*.

It can be shown that ergodicity is achieved when the actual concentration is close to its expectation. In a different way one could state that under ergodic conditions the variance $\sigma^2_{\overline{C}}$ of the mean concentration tends to zero (Dagan, 1987). The general expression of $\sigma^2_{\overline{C}}$ has been derived in previous studies (see, e.g. Dagan and Fiori, 1997; Fiori and Dagan, 2000), and the final result reads as

$$\sigma^2_{\overline{C}} = \left(\frac{C_0}{A_0}\right)^2 \int_{A_0}\int_{A_0}\iint d\mathbf{a}\, d\mathbf{b}\, d\mathbf{X}\, d\mathbf{Y}[f(\mathbf{X},\mathbf{Y},t;\mathbf{a},\mathbf{b}) - f(\mathbf{X},t;\mathbf{a})f(\mathbf{Y},t;\mathbf{b})], \tag{22}$$

being C_0 the (constant) initially injected solute concentration. In Eq. (22), $f(\mathbf{X},\mathbf{Y},t;\mathbf{a},\mathbf{b})$ represents the joint pdf of the trajectories $\mathbf{X}$ and $\mathbf{Y}$ of two particles starting at different positions $\mathbf{a}$ and $\mathbf{b}$. Similarly, $f(\mathbf{X},t;\mathbf{a})$ is the pdf of $\mathbf{X}$. The basic result (Eq. (22)) suggests a very simple way to assess the ergodicity attainment. Indeed, when the trajectories $\mathbf{X}$ and $\mathbf{Y}$ become uncorrelated it yields $f(\mathbf{X},\mathbf{Y},t;\mathbf{a},\mathbf{b}) \to f(\mathbf{X},t;\mathbf{a})f(\mathbf{Y},t;\mathbf{b})$, and from Eq. (22) one has $\sigma^2_{\overline{C}} \to 0$. Now, at the σ^2_ε-order the fluctuation $\overline{X}'_r$ is proportional to the velocity fluctuation $u^{(1)}_r$, and one may look at the pattern of the velocity correlation to establish when (and how) transport becomes ergodic. By recalling the analysis of the velocity covariance (see previous section) we argue that, unlike mean uniform flows, ergodicity can be achieved even for a relatively (as compared with I^2) small A_0 as well as at large distances from the source.

To study the tendency to the ergodicity in a more quantitative manner, we shall refer to the condition $\mathcal{R}_{rr} \to 0$ (an extensive discussion on this issue can be found in Rubin, 2003). The computation of $\mathcal{R}_{rr}$ is related (see Eq. (21)) to that of the fluctuation $\overline{X}'_r$ which, at the first order approximation in σ^2_ε, is given by (Indelman and Rubin, 1996):

$$\langle u(R)\rangle = \frac{d}{dt}R = \frac{Q}{2\pi n R}, \qquad \frac{d}{dt}\overline{X}'_r = u^{(1)}_r + \overline{X}'_r \frac{\partial}{\partial R}\langle u(R)\rangle. \tag{23}$$

The first of (Eq. (23)) is solved straightforwardly with zero initial condition, i.e.

$$R(t) = \left(\frac{Qt}{\pi n}\right)^{1/2}. \tag{24}$$

To solve the second equation in Eq. (23), it is convenient to switch to R as independent variable, and to make use of Eq. (24) to yield

$$\overline{X}_{r'}(R,a) = \frac{2\pi n}{QR}\int_a^R d\mathrm{x}\, \mathrm{x}^2 u^{(1)}_r(\mathrm{x}) \qquad (\mathbf{a} \in A_0). \tag{25}$$

The trajectory variance is calculated as

$$\mathrm{X}_{rr}(R,a,b) = \langle \overline{X}_{r'}(R;a)\overline{X}_{r'}(R;b)\rangle = \mathrm{X}\left(\frac{2\pi n}{QR}\right)^2 \int_a^R\int_b^R d\mathrm{x}dy(\mathrm{x}y)^2 u_{rr}(\mathrm{x},y), \tag{26}$$

and concurrently Eq. (21) (for a circular input zone $A_0 = \pi\ell^2$) writes as:

$$\mathcal{R}_{rr}(R,\ell) = \left(\frac{4\pi n}{QR\ell^2}\right)^2 \int_0^\ell\int_0^\ell da db\, ab\int_a^R\int_b^R dxdy(xy)^2 u_{rr}(x,y). \tag{27}$$

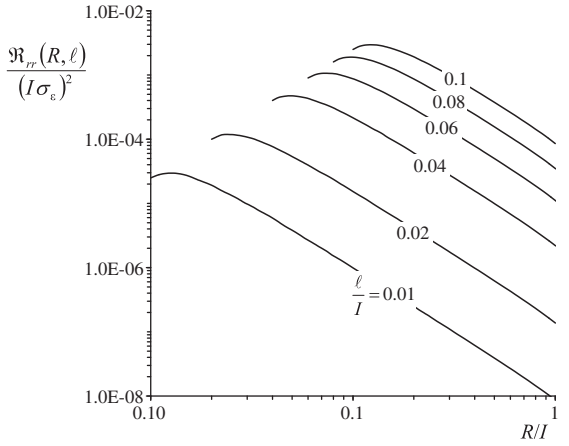

Fig. 3. Dependence of the dimensionless variance $\frac{\mathcal{R}_{rr}(R,\ell)}{(I\sigma_\varepsilon)^2}$ of the plume centroid upon the scaled distance $\frac{R}{I}$, and several values of the relative characteristic radius $\frac{\ell}{I}$.

The dimensionless variance $\frac{\mathcal{R}_{rr}(R,\ell)}{(I\sigma_\varepsilon)^2}$ has been depicted in Fig. 3 versus $\frac{R}{I}$, and different values of the relative radius $\frac{\ell}{I}$ of the input zone. The main feature is two-fold. Close to the source $\mathcal{R}_{rr}$ is relatively large since velocities there are highly correlated (see also Fig. 2). As a consequence, transport is non-ergodic at the source. However, after one integral scale $\mathcal{R}_{rr}$ drastically reduces, and therefore by such a distance transport can be practically regarded as ergodic. In addition, the rate of approaching ergodicity increases as $\frac{\ell}{I}$ reduces. This is understandable since, when the release area is small, solute particles become uncorrelated soon.

Summarizing, even if transport is non-ergodic at the source, we can regard it as ergodic already at radial distances greater than one integral scale. Since in most of the practical applications this is the case (as it will be also clearer in the next section), it is reasonable to model macrodispersion by means of $X_{rr}(R,0)$. To compute this latter (that for brevity hereafter we shall denote as $X_{rr}(R)$), we note that it can be rewritten (see Eq. (9)) as

$$X_{rr}(R) = 4X^{(\infty)}_{rr}(R) + 3\widetilde{X}_{rr}(R), \tag{28}$$

$$\mathrm{X}^{(\infty)}_{rr}(R) = \frac{\sigma^2_\varepsilon}{3} R\int_0^R d\mathrm{x}\,\rho_\varepsilon(\mathrm{x})\left(\frac{\mathrm{x}^3}{R^3} - 3\frac{\mathrm{x}}{R} + 2\right) \tag{29}$$

$$\widetilde{\mathrm{X}}_{rr}(R) = \left(\frac{\sigma_\varepsilon}{R}\right)^2 \int_0^R\int_0^R d\mathrm{x}dy\,(\mathrm{x}y)^2\Psi(\mathrm{x},y). \tag{30}$$

The usefulness of the decomposition (Eq. (28)) relies on the fact that in this way we can clearly distinguish: i) the contribution $X^{(\infty)}_{rr}(R)$ to macrodispersion in the far field, and ii) the term $\widetilde{X}_{rr}(R)$ due to the fluctuations of the head-gradient. In a different way, we could say that by adopting the approximation suggested by Indelman and Dagan

(1999), the computation of $X_{rr}(R)$ would result in retaining $X_{rr}^{(\infty)}(R)$, solely. The evaluation of $X_{rr}^{(\infty)}(R)$ is straightforward once the shape of the autocorrelation ρ_ε is chosen. Thus, it yields

$$X_{rr}^{(\infty)}(R) = \frac{1}{3}\left(\frac{\sigma_\varepsilon}{R}\right)^2\left[2R^3 - 3R^2 + 6 - 6(1+R)\exp(-R)\right] \quad (31)$$

for exponential, and

$$X_{rr}^{(\infty)}(R) = \frac{1}{6}\left(\frac{\sigma_\varepsilon}{\pi R}\right)^2\left[\pi R\overline{R}^2\,\mathrm{erf}(\overline{R}) - 3\overline{R}^2 + 1 + 2\left(\overline{R}^2 - \frac{1}{2}\right)\exp\left(-\overline{R}^2\right)\right] \quad (32)$$

(with $\overline{R} = \frac{\sqrt{\pi}}{2}R$) for Gaussian ρ_ε, respectively. The computation of $\widetilde{X}_{rr}(R)$ is achieved by means of a numerical quadrature.

We have depicted in Fig. 4 the dimensionless trajectory variance (continuous line) $\dfrac{X_{rr}(R)}{(I\sigma_\varepsilon)^2}$ versus the normalized distance $\dfrac{R}{I}$ for Gaussian autocorrelation. The same behavior is observed in the case of exponential ρ_ε. To emphasize the difference with the approximation of Indelman and Dagan (1999), we have also shown (dot line) the term $X_{rr}^{(\infty)}(R)$. Finally, for comparison purposes, the trajectory variance characterizing transport in mean uniform flow, i.e.

$$X^{(\mathrm{unif})}(R) = (I\sigma_\varepsilon)^2 R\int_0^\infty \frac{dx}{x^3}\left[2J_1(x) - xJ_0(x)\right]\left[\mathrm{erfc}(\overline{x}) + \frac{\overline{x}}{\sqrt{\pi}}\mathrm{Ei}\left(-\overline{x}^2\right)\right] \quad (33)$$

(where we have set $\overline{x} = \dfrac{x}{\sqrt{\pi R}}$) is also drawn (dashed line). As the tracer body invades the porous medium, X_{rr} grows monotonically with the distance. At short distances X_{rr} exhibits a nonlinear dependence, whereas for R large enough X_{rr} grows linearly. It is interesting to observe that the transitional regime is much more persistent for $X_{rr}(R)$ than that for $X_{rr}^{(\infty)}(R)$, since retaining only $X_{rr}^{(\infty)}(R)$ implies neglecting the impact of the head-gradient fluctuations (which are still relevant). For $R>20I$ the influence of the fluctuations of the head-gradient is practically negligible, and transport has reached its asymptotic (Fickian) regime. This represents an important issue in practical applications such as the use of tracer tests to identify the formation statistical structure (see discussion in Fernàndez-Garcia et al., 2005).

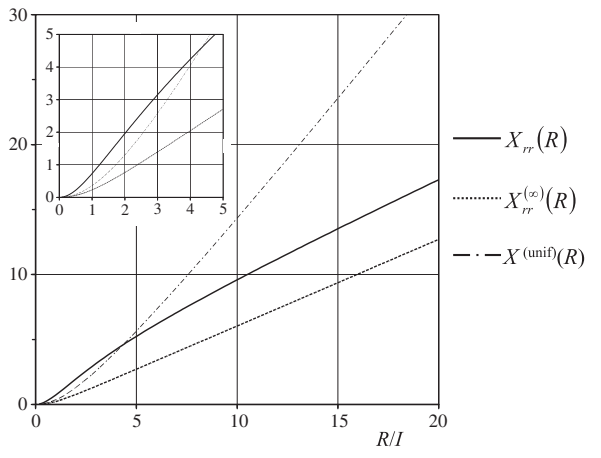

Fig. 4. Trajectory variance $X_{rr}(R)$ for mean radial flow as function of the travel distance $\frac{R}{I}$ (Gaussian autocorrelation of ε).

Due to the nonuniformity of the mean radial flow, there is a significant difference as compared with the case of mean uniform flow depending whether one considers small or large distances from the source. This is explained by recalling that, while $\langle u\rangle$ is constant in mean uniform flows, it decays like r^{-1} in a radial configuration. As a consequence, at small distances (say for $R<5I$) spreading due to source-flows is more pronounced as compared with that due to mean uniform flows. At large distances (say for $R>5I$) the behavior is reversed since now velocities generated by the source flow are quite small, thus causing a much smaller spreading. As a consequence, the distance $R\simeq 5I$ can be considered as the onset distance of the approximation of Indelman and Dagan (1999). One important consequence of such a kinematical picture is that the macrodispersivity tends to a (constant) value smaller than that in mean uniform flow (see discussion in Indelman and Dagan, 1999).

Another quantity of interest in applications is the *breakthrough curve* (BTC) recovered at any radial position. For a pulse injection, the BTC is proportional to the probability distribution function f of the trajectory $\overline{X}_r$. At the σ_ε^2-approximation the fluctuation $\overline{X}_r'$ is proportional (see Eq. (25)) to the velocity fluctuation $u_r^{(1)}$, and concurrently to the normally distributed RSF ε. Thus, the particle trajectory f is normal, i.e.

$$f(r,t) = \frac{1}{2\pi X_{rr}(t)}\exp\left\{-\frac{[r-R(t)]^2}{2X_{rr}(t)}\right\}. \quad (34)$$

in the context of the adopted approximations, and the mean concentration is Gaussian. In addition, it is reminded that $\overline{X}_r$ tends asymptotically to normality by virtue of the central limit theorem. The usefulness of the BTC concept in the applications will be illustrated next.

4. Analysis of a forced-gradient tracer test

It is worth to show the application of our model to real data. Unfortunately, there are very few field scale forced tracer tests, and most lack the amount of data required for validation purposes. However, we found in the literature (Fernàndez-Garcia et al., 2004) a *divergent flow tracer test* (DFTT) suitable for comparison purposes. Although the test aquifer was artificially packed, it exhibits statistical properties resembling those found in some actual field settings (see Gelhar et al., 1992).

The DFTT is described into details by Fernàndez-Garcia et al. (2004). For the sake of completeness, the test (whose experimental set-up is sketched in Fig. 5) is described briefly herein. A sand tank (243.8 cm long, 121.9 cm wide, and 63.5 cm high) was constructed in the laboratory. The heterogeneity structure was artificially created by packing (for a complete description of the methodology see Chao et al., 2000; Fernàndez-Garcia et al., 2004) five different types of sands (the porosity n ranged between 0.35 and 0.42). The final arrangement of sand packs was such that the log-conductivity $Y=\ln K$ is a RSF with (geometric) mean and variance equal to $K_G = exp\langle Y\rangle = 116.7\dfrac{m}{d}$ and $\sigma_Y^2 = 1.79$, respectively. The autocorrelation of Y was characterized by

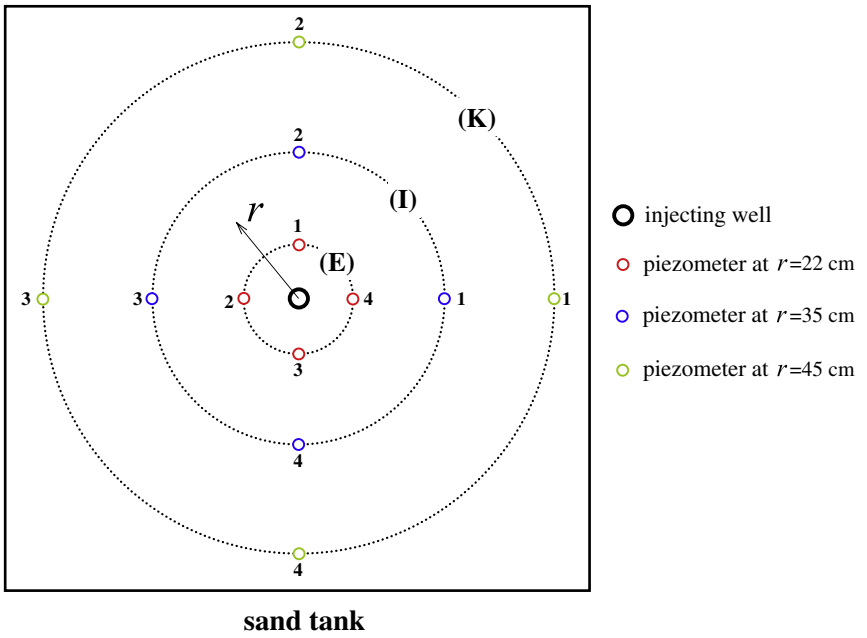

Fig. 5. Sketch of the experimental set-up of the *divergent flow tracer test* (plan view) carried out by Fernàndez-Garcia et al. (2004).

anisotropic structure with horizontal, and vertical integral scales equal to 10 cm and 3 cm, respectively.

A fully penetrating well, located at the center of the aquifer in conjunction with a peristaltic pump, was used to force the flow at a constant volumetric rate $\left(95\frac{\mathrm{mL}}{\mathrm{min}}\right)$. After reaching steady state conditions, a pulse of lithium bromide (LiBr) was added into the injection well over a period of 5 min. Concentrations with time were monitored into three batteries (each one formed by four piezometers) located at: i) $r=22$cm (battery E), ii) $r=35$cm (battery I), and iii) $r=45$cm (battery K) from the injecting well (Fig. 5).

The configuration of the field test of Fernàndez-Garcia et al. (2004) differs from the assumptions underlying our model in two respects. First, our model deals with a two-dimensional formation, whereas the experimental aquifer is of three-dimensional nature, and secondly our methodology applies to formations characterized by a relatively small variance, whereas in the experiment of Fernàndez-Garcia et al. (2004) the variance of Y is 1.79. However, as it will be immediately clear, such conditions only apparently prevent the use of our model.

As for the first issue, it is well known that only under conditions of uniformity along the depth would a two-dimensional model yield an accurate interpretation of a three-dimensional solute transport. However, in many practical problems we face formations whose areal dimensions are greater than the depth (Shapiro and Cvetkovic, 1990). In this case, although transport cannot be strictly considered as two-dimensional, it is still possible to adopt a two-dimensional approach. Such an approach is warranted when the *Dupuit*'s assumption holds. In particular, Severino et al. (2008) have shown that radial flows in heterogeneous porous formations exhibit stream lines that are essentially horizontal. As a consequence, the *Dupuit*'s assumption can be adopted in such a case.

As for the second issue, we need to relate the statistical structure of the log-conductivity Y to that pertaining to the transmissivity T. We use here the up-scaling methodology developed by Shapiro and Cvetkovic (1990), and Tartakovsky et al. (2000) relying on the definition of transmissivity as depth-averaged conductivity along the formation thickness b. In such a sense, the transmissivity statistical structure has to be sought in an *effective* manner, and not as a medium property. In a different way, we could say that the three-dimensional nature of the hydraulic conductivity K is encompassed in that of the effective transmissivity T. By skipping the analytical derivations (which can be found in Shapiro and Cvetkovic, 1990; and Tartakovsky et al., 2000), one ends up with the fundamental relationship

$$C_T(\mathrm{x}) = 2(I_v K_G)^2 \exp\left(\sigma_Y^2\right) \int_0^{b/I_v} d\alpha \left(\frac{b}{I_v} - \alpha\right) \left\{\exp\left[\sigma_Y^2 \rho_Y(\mathrm{x},\alpha)\right] - 1\right\}, \tag{35}$$

which shows in a clear manner how the three-dimensional statistical structure of $Y=lnK$ is up-scaled to obtain that of T. In Eq. (35) I_v and ρ_Y represent the vertical integral scale, and the autocorrelation function of Y, respectively. The variance σ_T^2 of the transmissivity is obtained from Eq. (35) by taking $\mathrm{x}=0$.

By accounting for data as well as the experimental variogram of Fernàndez-Garcia et al. (2004), the variance σ_ε^2 of the transmissivity fluctuation is 0.38 (which corresponds to $\sigma_{\ln T}^2=0.32$), and therefore allowing for the use of the perturbation approach. The integral scale I is 11 cm. Because the transmissivity T is up-scaled, it is important to check its stationarity. Toward this aim, we refer to Fig. 1 in Shapiro and Cvetkovic (1990) (or alternatively to Fig. 2 in Tartakovsky et al., 2000) with $\frac{b}{I_v} = \frac{63.5\mathrm{cm}}{3\mathrm{cm}} = 21.2$ and $\sigma_Y^2=1.79$. It is immediately seen that T can be regarded as a stationary RSF.

Before continuing, it is worth to discuss a few issues. First, in the experiment of Fernàndez-Garcia et al. (2004), and similarly in other field scale tests (e.g. Molz et al., 1986; Yeh et al., 1995), the plume detection is carried out by piezometers parallel to the well. Thus, concentration is averaged over the vertical by measuring it after mixing in the piezometer (see also discussion in Kreft and Zuber, 1978). As a consequence, the BTC is a quantity which is uniform along the depth, and therefore it represents the proper benchmark to be used in our case for validating purposes. Second, it is well known that two-dimensional modelling of well-type flows may lead to different results close to the injection zone (see discussion in Indelman et al., 1996). However, the difference between two and three-dimensional modelling of source-flows is mainly felt at relatively (generally one integral scale) small distances from the source (Severino et al., 2008). Thus, if the plume is detected at distances greater than a few integral scales (like in the case of the DFTT of Fernàndez-Garcia et al., 2004), the issue of the space dimensionality represents an unwarranted complication. Nevertheless, many studies have underlined the usefulness of two-dimensional modeling of flow and transport in radial configurations (e.g. Neuman et al., 2004; Riva et al., 2001; Riva et al., 2006; Sanchez-Vila, 1997). Last, it is important to observe here that the geometrical configuration of the DFTT of Fernàndez-Garcia et al. (2004) allows to regard transport as ergodic. In fact, the closest battery of sampling piezometers was at $\frac{R}{I}=2$ (see Fig. 5), and because $\frac{\ell}{I}=\frac{0.75\text{cm}}{11\text{cm}}=0.07$ we conclude (see Fig. 3) that transport can be considered as ergodic.

In Fig. 6(a–c) the analytical solution is compared to the solute BTCs measured in the transport experiment of Fernàndez-Garcia et al. (2004). More precisely, in Fig. 6a we show the normalized BTCs (thin lines with discrete symbols) inside the four piezometers (E_1, E_2, E_3, and E_4) at the radial distance $r=22$ cm (see Fig. 5), together with the average (thick dashed line), and the analytical (thick solid line) BTC. In the same manner, we compare in Fig. 6b,c the model and data at the other radial distances, i.e. $r=35$ and 45 cm. It is clearly seen that, although the plume is ergodic, local BTCs at any radial distance may result quite different one from each other. In fact, since solute particles are uncorrelated, it is natural to expect that the BTCs at the piezometers (representing single realizations of the mean BTC) will result different. Nevertheless, it is interesting to observe that the average BTC is in relatively good agreement with the analytical one. The discrepancy is mainly addressed to the fact that the average is computed by using only four local (i.e. single realizations) BTCs. A further improvement can be reasonably achieved by accounting for pore-scale dispersion. Other reasons which may explain the disagreement between the model and the average BTC pertain to the uncertainty in the estimated hydraulic properties. Indeed, even if the up-scaling procedure allows one to consider a relatively small variance, it nevertheless affects the uncertainty in the BTC. Finally, it is worth reminding that the proposed comparison relies only upon statistical formation properties, and therefore without any fitting against concentration data. Thus, Fig. 6a–c demonstrate that the proposed stochastic model captures the salient features of the transport experiment of Fernàndez-Garcia et al. (2004).

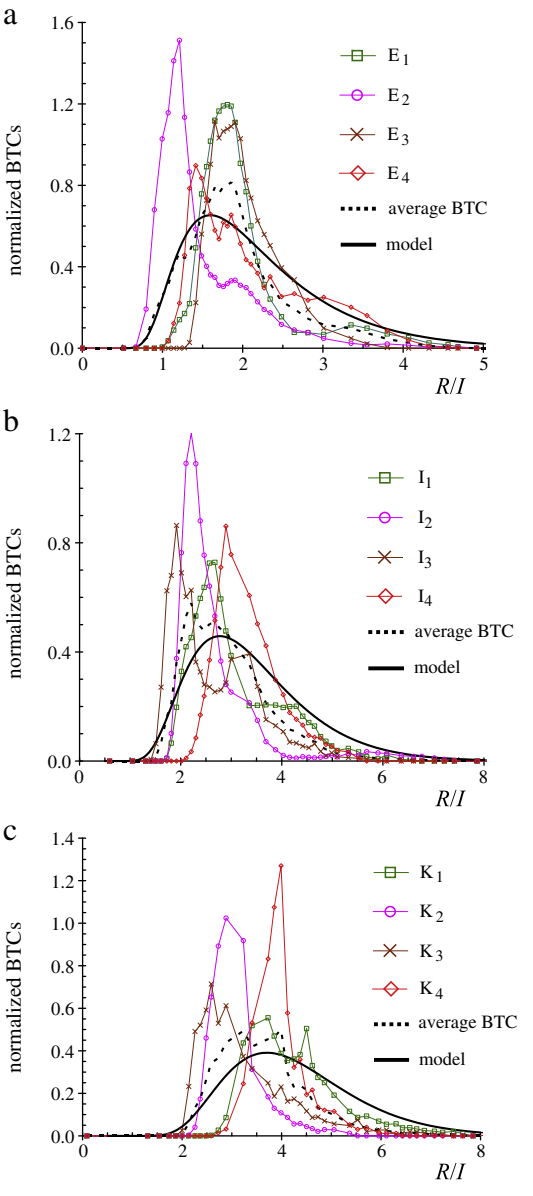

Fig. 6. Comparison between theoretical (thick solid line), average (thick dashed line), and single realizations (thin lines with discrete symbols) normalized BTCs at: a) $\frac{r}{I}=\frac{22\text{cm}}{11\text{cm}}$, b) $\frac{r}{I}=\frac{35\text{cm}}{11\text{cm}}$, and c) $\frac{r}{I}=\frac{45\text{cm}}{11\text{cm}}$.

5. Concluding remarks

The problem investigated here is that of tracer macrodispersion into a radial flow configuration. The plume spreads due to the velocity fluctuations that are caused by the spatial variability of the transmissivity *T*. The difficulty of such a problem stems from the fact that, unlike the common natural gradient conditions, the flow pattern is nonuniform in mean.

To reduce the mathematical complexity, while keeping the most relevant features of the problem at stake, a few simplifying assumptions have been adopted. Pore-scale dispersion is neglected, and a first order approximation in the variance σ_ε^2

of the fluctuation (Eq. (3)) is employed to evaluate the velocity covariance. This problem was analytically tackled in the past (Indelman and Dagan, 1999) by neglecting in the velocity covariance the contribution of the head-gradient fluctuations. Such an approximation is bound to become accurate at large distances from the release zone. However, in many practical applications (e.g. Chao et al., 2000; Fernàndez-Garcia et al., 2004) BTCs are monitored (due to logistic as well as instrumental limitations) at distances relatively short (only a few integral scales from the injection zone), *de facto* preventing the applicability of such an approximation.

In the present paper, we have derived an analytical expression for spatial moments that is valid at σ_ε^2-order. Overall, both the centroid trajectory and radial spatial moments are RSFs at the injection zone. As matter of fact, at the very early stages transport is non ergodic. However, it is shown that ergodicity is achieved after a relatively short transitional regime. This is due to the high local fluid velocities at the source, which enable solute particles to become uncorrelated very soon. A striking result, that totally differs from the case of uniform mean flows, is that the ergodic hypothesis is fulfilled if the length scale ℓ of the release zone is small as compared with the integral scale I of the transmissivity. Under ergodic conditions, the structure and evolution of $X_{rr}(R)$ is discussed. One interesting feature is that the transitional regime between the early and large distances is much more persistent for $X_{rr}(R)$ as compared with that based on the approximation of Indelman and Dagan (1999). This is due to the impact of the covariances involving the head-gradient, which in the region of the order of five integral scales (being typical of the sampling locations) are still affecting the tracer dispersion.

Beside the theoretical interest, results of the present paper are also useful for practical applications. Indeed, the model is tested against a forced-gradient experiment (Fernàndez-Garcia et al., 2004). Although the experimental conditions do not fit exactly the assumptions underlying our model, we found (after up-scaling the hydraulic conductivity) that the model captures the global behavior of the plume at early distances, although some differences are still observed. The current study may be extended in many directions, analyzing the same problem by means of temporal moments, and accounting for pore-scale dispersion as well as the nonstationarity of T. Most of these challenging tasks are topics of ongoing research.

Acknowledgments

We are deeply indebted to Daniel Fernàndez-Garcia (Polytechnic University of Valencia, Spain), Tissa H. Illangasekare (Colorado School of Mines, USA), and the US Army Research Office for providing us the complete data-set concerning the DFTT. We are very grateful to Daniel Fernàndez-Garcia, and two anonymous reviewers for their thorough and helpful comments which have significantly improved the early version of the manuscript. Suggestions from Gerardo Toraldo (University of Naples, Italy) and Gabriella Pisanti are kindly acknowledged.

This study was supported by the grant: *Methods for monitoring, predicting and controlling soil and groundwater pollution processes due to non-point agricultural sources* (#MIUR 2007WA23ZC).

Appendix A. Derivation of the velocity covariance

The velocity covariance u_{rr} is determined by means of $C_{\varepsilon H}$, and C_{E_r} (see Eqs. (9–11)). To compute these latter, we first calculate the head fluctuation. Thus, from Eq. (7) and by using the relationship $\frac{\partial}{\partial x_m} = \frac{x_m}{x}\frac{d}{dx}$, one has

$$H^{(1)}(\mathbf{r}) = \frac{Q}{T_A}\int_\Omega \frac{d\bar{\mathbf{r}}}{(2\pi)^2}\varepsilon(\bar{\mathbf{r}})\frac{\bar{\mathbf{r}}\cdot(\bar{\mathbf{r}}-\mathbf{r})}{(\bar{r}|\bar{\mathbf{r}}-\mathbf{r}|)^2}. \tag{36}$$

The cross-covariance $C_{\varepsilon H}$ is calculated by multiplying $\varepsilon(\mathbf{r}')$ by (36) evaluated in $\mathbf{r}''\neq\mathbf{r}'$, and subsequently taking the expectation to get

$$C_{\varepsilon H}(\mathbf{r}',\mathbf{r}'') = \frac{Q}{T_A}\left(\frac{\sigma_\varepsilon}{2\pi}\right)^2\int_\Omega d\bar{\mathbf{r}}\rho(\bar{r})\frac{(\mathbf{r}'-\bar{\mathbf{r}})\cdot(\mathbf{r}'-\mathbf{r}''-\bar{\mathbf{r}})}{(|\mathbf{r}'-\bar{\mathbf{r}}||\mathbf{r}'-\mathbf{r}''-\bar{\mathbf{r}}|)^2}. \tag{37}$$

Switching to polar coordinates $\bar{\mathbf{r}} = \bar{\mathbf{r}}(\bar{r},\theta)$

$$C_{\varepsilon H}(r',r'') = \frac{Q}{T_A}\left(\frac{\sigma_\varepsilon}{2\pi}\right)^2\int_0^\infty d\bar{r}\bar{r}\rho(\bar{r})\int_0^{2\pi}d\theta\frac{\bar{r}^2+r'(r'-r'')-\bar{r}(2r'-r'')\cos\theta}{\beta(r')\beta(r'-r'')} \tag{38}$$

$$\beta(a) = \bar{r}^2 + a^2 - 2a\bar{r}\cos\theta. \tag{39}$$

integrating over the angle

$$\int_0^{2\pi}d\theta\frac{\bar{r}^2+r'(r'-r'')-\bar{r}(2r'-r'')\cos\theta}{\beta(r')\beta(r'-r'')} = 2\pi\frac{h(\bar{r}-|r'-r''|)-h(r'-\bar{r})}{\bar{r}^2-r'(r'-r'')} \tag{40}$$

(h is a Heaviside function defined as: $h(x)=0$ for $x<0$, $h(x)=1/2$ for $x=0$, and $h(x)=1$ for $x>0$), and substituting into Eq. (38), leads to Eq. (13).

The computation of the head-gradient covariance C_{E_r} is achieved in a similar manner. We start with the derivation of the head covariance C_H by employing the definition, i.e.

$$C_H(\mathbf{r}',\mathbf{r}'') = \left\langle H^{(1)}(\mathbf{r}')H^{(1)}(\mathbf{r}'')\right\rangle = \frac{Q}{T_A}\int_\Omega\frac{d\bar{\mathbf{r}}}{(2\pi)^2}\frac{\bar{\mathbf{r}}\cdot(\bar{\mathbf{r}}-\mathbf{r}')}{(\bar{r}|\bar{\mathbf{r}}-\mathbf{r}'|)^2}C_{\varepsilon H}(\bar{\mathbf{r}},\mathbf{r}''). \tag{41}$$

Like before, we switch to polar coordinates

$$C_H(r',r'') = \frac{Q}{T_A}\int_0^\infty\frac{d\bar{r}}{(2\pi)^2}C_{\varepsilon H}(\bar{r},r'')\int_0^{2\pi}d\theta\frac{\bar{r}-r'\cos\theta}{\beta(r'),} \tag{42}$$

and compute the quadrature over the angle, i.e. $\int_0^{2\pi}d\theta\frac{\bar{r}-r'\cos\theta}{\beta(r')} = 2\pi\bar{r}h(\bar{r}-r')$, to get

$$C_H(r',r'') = \chi^{-1}\int_{r'}^\infty\frac{d\bar{r}}{\bar{r}}C_{\varepsilon H}(\bar{r},r''). \tag{43}$$

The head-gradient covariance (Eq. (16)) is easily obtained from Eq. (43) after carrying out the derivatives with respect to r' and r''.

References

Chao, C.-H., Rajaram, H., Illangasekare, T.H., 2000. Intermediate scale experiments and numerical simulations of transport under radial flow in a two-dimensional heterogeneous porous medium. Water Resour. Res. 36, 2869–2884.

Cvetkovic, V., Dagan, G., 1994. Transport of kinetically sorbing solute by steady random velocity in heterogeneous porous formations. J. Fluid Mech. 265, 189–215.

Dagan, G., 1987. Theory of solute transport by groundwater. Annu. Rev. Fluid Mech. 19, 183–215.

Dagan, G., 1990. Transport in heterogeneous formations: spatial moments, ergodicity and effective dispersion. Water Resour. Res. 26, 1281–1290.

Dagan, G., Fiori, A., 1997. The influence of pore-scale dispersion on concentration statistical moments in transport through heterogeneous aquifers. Water Resour. Res. 33, 1595–1606.

Fernàndez-Garcia, D., Illagasekare, T.H., Rajaram, H., 2004. Conservative and sorptive forced-gradient and uniform flow tracer tests in a three-dimensional laboratory test aquifer. Water Resour. Res. 40, W10103. doi:10.1029/2004WR003112.

Fernàndez-Garcia, D., Illagasekare, T.H., Rajaram, H., 2005. Differences in the scale dependence of dispersivity and retardation factors estimated from forced-gradient and uniform flow tracer tests in three-dimensional physically and chemically heterogeneous porous media. Water Resour. Res. 41, W03012. doi:10.1029/2004WR003125.

Fiori, A., Dagan, G., 2000. Concentration fluctuations in aquifer transport: a rigorous first-order solution and applications. J. Contam. Hydrol. 45, 139–163.

Fiori, A., Indelman, P., Dagan, G., 1998. Correlation structure of flow variables for steady flow toward a well with application to highly anisotropic heterogeneous formations. Water Resour. Res. 34, 699–708.

Gelhar, L.W., Welty, C., Rehfeldt, K., 1992. A critical review of data on field-scale dispersion aquifers. Water Resour. Res. 28, 1955–1974.

Indelman P., 2001. Steady-State Source Flow in Heterogeneous Porous Media. Transp. Porous Media 45, 105–127.

Indelman, P., Abramovich, B., 1994. Nonlocal properties of nonuniform averaged flows in heterogeneous media. Water Resour. Res. 30, 3385–3393.

Indelman, P., Dagan, G., 1999. Solute transport in divergent radial flow through heterogeneous porous media. J. Fluid Mech. 384, 159–182.

Indelman, P., Rubin, Y., 1996. Solute transport in nonstationary velocity fields. Water Resour. Res. 32, 1259–1267.

Indelman, P., Fiori, A., Dagan, G., 1996. Steady flow toward wells in heterogeneous formations: mean head and equivalent conductivity. Water Resour. Res. 32, 1975–1983.

Kitanidis, P., 1988. Prediction by the method of moments of transport in a heterogeneous formation. J. Hydrol. 102, 453–473.

Kreft, A., Zuber, A., 1978. On the physical meaning of the dispersion equation and its solution for different initial and boundary conditions. Chem. Eng. Sci. 33, 1471–1480.

Lessoff, S.C., Indelman, P., 2004. Stochastic determination of three-dimensional capture zones for a fully penetrating well. Water Resour. Res. 40, W03508. doi:10.1029/2003WR002703.

Molz, F.J., Goven, O., Melville, J.G., Crocker, R.D., Matteson, K.T., 1986. Performance, analysis, and simulation of a two-well tracer test at the mobile site. Water Resour. Res. 22, 1031–1037.

Morales-Casique, E., Neuman, S.P., Guadagnini, A., 2006. Non-local and localized analyses of non-reactive solute transport in bounded randomly heterogeneous porous media: theoretical framework. Adv. Water Resour. 29, 1238–1255. doi:10.1016/j.advwatres.2005.10.002.

Neuman, S.P., Guadagnini, A., Riva, M., 2004. Type-curve estimation of statistical heterogeneity. Water Resour. Res. 40, W04201. doi:10.1029/2003WR002405.

Ptak, T., Piepenbrink, M., Martac, E., 2004. Tracer tests for the investigation of heterogeneous porous media and stochastic modelling of flow and transport: a review of some recent developments. J. Hydrol. 294, 122–163.

Riva, M., Guadagnini, A., Neuman, S.P., Franzetti, S., 2001. Radial flow in a bounded, randomly heterogeneous aquifer. Transp. Porous Media 45, 139–193.

Riva, M., Sánchez-Vila, X., Guadagnini, A., De Simoni, M., Willmann, M., 2006. Travel time and trajectory moments of conservative solutes in two-dimensional convergent flows. J. Cont. Hydrol. 82, 23–43.

Rubin, Y., 2003. Applied Stochastic Hydrogeology. Oxford University Press.

Sanchez-Vila, X., 1997. Radially convergent flow in heterogeneous porous media. Water Resour. Res. 33, 1633–1641.

Severino, G., Santini, A., Sommella, A., 2008. Steady flows driven by sources of random strength in heterogeneous aquifers with application to partially-penetrating wells. Stoch. Environ. Res. Risk Assess. 22. doi:10.1007/s00477-007-0175-5.

Shapiro, A.M., Cvetkovic, V.D., 1990. A comparison of two- and three-dimensional stochastic models of regional solute movement. Transp. Porous Media 5, 1–25.

Shvidler, M.I., 1966. The source-type solution of the problem of unsteady flow in random porous media. Fluid Dyn. 95–98.

Tartakovsky, D.M., Guadagnini, A., Guadagnini, L., 2000. Effective hydraulic conductivity and transmissivity for heterogeneous aquifers. Math. Geol. 32, 751–759.

Yeh, T.-C.J., Mas-Pla, J., Williams, T.M., McCarthy, J.F., 1995. Observation and three dimensional simulation of chloride plumes in a sandy aquifer under forced-gradient conditions. Water Resour. Res. 31, 2141–2157.

Zhang, D., 2002. Stochastic Methods for Flow in Porous Media. Academic Press.